ISSN 1063-7826, Semiconductors, 2012, Vol. 46, No. 9, pp. 1126–1134. © Pleiades Publishing, Ltd., 2012.

SPECTROSCOPY, INTERACTION WITH RADIATION

Velocity-Direction Dependent Transmission Coefficient of Electron through Potential Barrier Grown on Anisotropic Semiconductor[1]

Chun-Nan Chen[a]^, Sheng-Hsiung Chang[b], Wei-Long Su[c], Jen-Yi Jen[a], and Yiming Li[d]

[a]*Quantum Engineering Laboratory, Department of Physics, Tamkang University, Tamsui, Taipei 251, Taiwan*

^*e-mail: quantum@mail.tku.edu.tw*

[b]*Department of Optoelectronic Engineering, Far-East University, Hsin-Shih Town, Tainan, Taiwan*

[c]*Department of Digital Mulitimedia Technology, Lee-Ming Institute of Technology, Tai-Shan, Taipei 24305, Taiwan*

[d]*Department of Electrical Engineering, National Chiao Tung University, Hsinchu 300, Taiwan*

Received November 14, 2011; in final form, March 6, 2012

Abstract—In contrast to the usual wavevector dependent transition coefficients, the velocity-direction dependent transition coefficients of an incident electron are calculated. Through a potential barrier grown on anisotropic semiconductors, the transition coefficients of an incident electron are calculated in all valleys and incident-directions. In the anisotropic semiconductor, the mathematical expressions of the electron wavevector are also derived in the framework of the incident-angle and incident-energy parameters.

DOI: 10.1134/S1063782612090060

1. INRODUCTION

Metal-oxide-semiconductor field-effect transistors (MOSFETs) constitute the fundamental building block of the present day complementary metal-oxide semiconductor technology. Current research in this field is largely geared towards improving MOSFET performance and increasing device density through aggressive scaling of their feature sizes [1, 2]. As MOSFET channel lengths approach few tens of nanometers, source-to-drain potential-barrier tunneling in these near-ballistic devices become important issues [3–5].

The effective-mass equation provides an accurate and easy to implement model Hamiltonian that does justice to the device band structure including quantum-mechanical size effects, and it describes the slowly varying envelope part of the underlying Bloch wave function [6–9]. The non-equilibrium Green's-function method provides a rigorous formulation of quantum transport in nano-scale devices [10–12]. Together in this study, the Green's-function formalism and effective-mass equation are used to describe transport in nano-scale potential-barrier tunneling both in the ballistic limit.

The popular problem in nano-scale transistors is the quantum transport through the source-to-drain potential barrier [3–5]. The aim of this study is: for an incident electron through a potential barrier grown on an anisotropic material, the velocity-direction dependent transition coefficients are seldom calculated in the previous articles which are in contrast to the usual wavevector dependent transition coefficient that will be formulated and calculated in this study [13, 14]. If the transmission coefficients as a function of the incident-electron angle are known, we can use these results as the design principle of geometry shape of device body and Ohm's contact to improve MOSFET performance.

Band-structure engineering in semiconductor devices is an essential activity when developing high-performance electronic devices [15]. The crystallographic orientation represents another crucial degree of freedom in the design of electronic devices. The advances in growth technologies now enable the growth of high-quality epitaxial layers on both (001)-oriented and non-(001)-oriented substrates. As alternatives to the conventional (001) orientation, the most widely used substrate orientations belong to the (11N)-oriented family, e.g., (111) and (110) [16, 17].

Silicon wafers are almost universally used by the semiconductor industry for MOS integrated circuit fabrication. Germanium is an attractive candidate for ultra fast MOS technology due to its potential for doubling electron mobility and quadrupling hole mobility in comparison to silicon [18, 19]. The proposed method in this study is suitable for the velocity-direction dependent transmission-coefficient calculation of the traditional and modern Si- or Ge-based transistors in the ballistic limit [20–25].

[1] The article is published in the original.

The study formulates the components of the wavevector on an anisotropic material as a function of incident-electron angle, and then the angle-dependent transmission coefficients of (001)-, (111)-, and (110)-oriented potential-barriers of Si and Ge samples are calculated.

2. THEORETICAL METHODS

In this study, we will discuss the transmission coefficient $T(E, \theta, \phi)$ of electron through a potential barrier grown on an anisotropic material (ellipsoidal valley) under non-normal incident. Furthermore, the transmission coefficient $T(E, \theta, \phi)$ is dependent on the energy (E) and angle (θ, ϕ) of the incident electron, and the angles θ and ϕ are the polar and azimuthal angles of the velocity direction of the incident electron relative to the structure coordinate system (x', y', z'), respectively. Note that **k** (wavevector of the incident electron) and **v** (velocity of the incident electron) are not necessarily parallel in an anisotropic material.

The (θ, ϕ) and (θ', ϕ') are the angles coordinate components of **v** and **k** which relatives to the system coordinate (x', y', z'), respectively, and they can be defined as follows

$$\theta = \tan^{-1}(\{v_{x'}^2 + v_{y'}^2\}^{1/2}/|v_{z'}|), \tag{1a}$$

$$\phi = \tan^{-1}(v_{y'}/v_{x'}), \tag{1b}$$

$$\begin{aligned}\mathbf{k} = k_{x'}\hat{x}' + k_{y'}\hat{y}' + k_{z'}\hat{z}' = k\sin\theta'\cos\phi'\hat{x} \\ + k\sin\theta'\sin\phi'\hat{y} + k\cos\theta'\hat{z}.\end{aligned} \tag{2}$$

Let the electron potential, $V(z)$, be a function of the growth-direction distance, z, then the Hamiltonian for the general ellipsoidal-valley can be expressed as [13, 14]

$$\begin{aligned}H_0 &= \frac{\eta^2}{2}\sum_{i,j=x,y,z} k_i\alpha_{ij}k_j + V(z) \\ &= \frac{\eta^2}{2}\sum_{i,j=x,y} k_i\beta_{ij}k_j + \frac{\eta^2}{2}\alpha_{zz}k'^2 + V(z),\end{aligned} \tag{3}$$

where $\mathbf{k}_{\|} = (k_x, k_y)$ and k_z denote the in-plane and growth-direction wave-vector relative to coordinate system (x, y, z), $\beta_{ij} = \alpha_{ij} - \alpha_{iz}\alpha_{jz}/\alpha_{zz}$ ($i, j = x, y$), and α_{ij} is the 3×3 reciprocal effective mass tensor by the in-plane rotation of azimuthal angle ($\phi - \pi/2$), which can be obtained by

$$\begin{bmatrix}\alpha_{xx} & \alpha_{xy} & \alpha_{xz} \\ \alpha_{yx} & \alpha_{yy} & \alpha_{yz} \\ \alpha_{zx} & \alpha_{zy} & \alpha_{zz}\end{bmatrix} = \mathbf{O}_3^T\begin{bmatrix}W_{x'x'} & W_{x'y'} & W_{x'z'} \\ W_{y'x'} & W_{y'y'} & W_{y'z'} \\ W_{z'x'} & W_{z'y'} & W_{z'z'}\end{bmatrix}\mathbf{O}_3 \tag{4}$$

with W_{ij} (with $i, j = x', y', z'$), as shown in Appendix A, and

$$\mathbf{O}_3 = \begin{bmatrix}\cos(\phi - \pi/2) & -\sin(\phi - \pi/2) & 0 \\ \sin(\phi - \pi/2) & \cos(\phi - \pi/2) & 0 \\ 0 & 0 & 1\end{bmatrix}.$$

Note that the coordinate system (x, y, z) can be obtained by the in-plane rotation of azimuthal angle ($\phi - \pi/2$) on the coordinate system (x', y', z') with $\hat{z} = \hat{z}'$. Furthermore, it is noted that the above expressions are instructive in that k_z is separated into two parts, namely ($-\gamma$) and (k'), (i.e., $k_z = k' - \gamma$ with $\gamma = (\alpha_{xz}k_x + \alpha_{yz}k_y)/\alpha_{zz}$) [13, 14]. In addition, the time-independent Schödinger equation, $H_0\Psi = E\Psi$, with constant potential, $V(z)$, has an eigen-function of

$$\begin{aligned}\Psi = [A_+\exp(+ik_z z) + A_-\exp(-ik_z z)] \\ \times \exp(ik_x x)\exp(ik_y y),\end{aligned} \tag{5a}$$

or

$$\begin{aligned}\Psi = [A_+\exp(+ik' z) + A_-\exp(-ik' z)] \\ \times \exp(-i\gamma z)\exp(ik_x x)\exp(ik_y y),\end{aligned} \tag{5b}$$

where A_+ and A_- are the amplitudes of the propagation in the positive and negative directions along the z-axis, respectively. Therefore, we can obtain

$$-\frac{\eta^2}{2}\alpha_{zz}\frac{d^2\zeta(z)}{dz^2} + \lambda(z)\zeta(z) = E\zeta(z) \tag{6}$$

with

$$\lambda(z) = \frac{\eta^2}{2}\sum_{i,j=x,y}\beta_{ij}k_i k_j + V(z)$$

and

$$\zeta(z) = A_+\exp(+ik' z) + A_-\exp(-ik' z).$$

Next, the Schrödinger equation for a potential profile with an arbitrary shape can be solved by using our

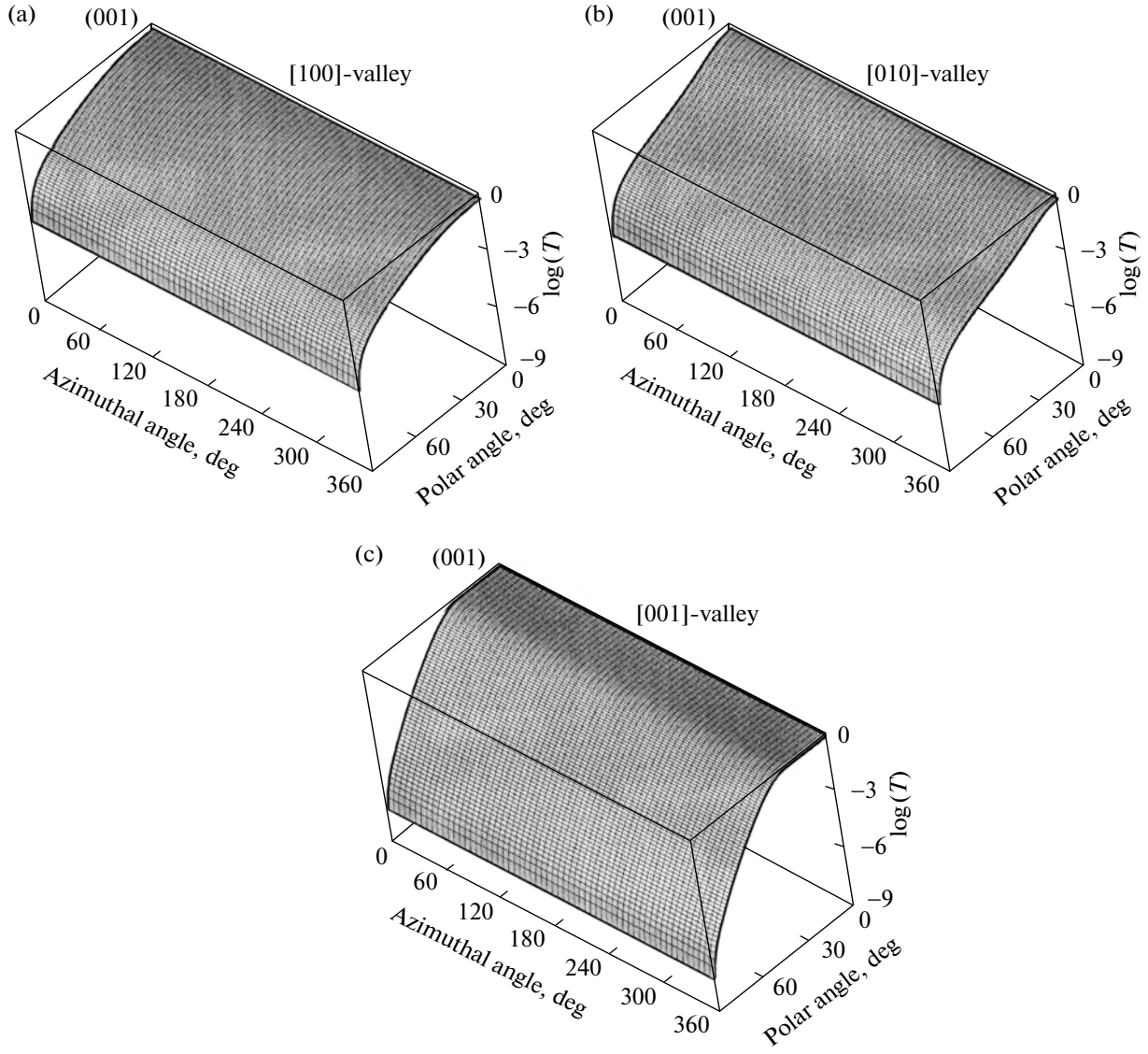

Fig. 1. Calculated transmission coefficients T in (001)-oriented Si rectangular potential barrier generated by incident electrons derived from (a) [100]-, (b) [010]-, and (c) [001]-valleys with different incident angles ($\theta = 0$–$90°$ and $\phi = 0$–$360°$).

previous calculating frameworks (the non-equilibrium Green's function or transfer-matrix methods) [12, 26].

The velocity in each direction of an incident electron can be defined as

$$v_i = \frac{1}{\theta}\frac{\partial E}{\partial k_i} \quad i = x, y, z, \tag{7}$$

which can be written as follows

$$v_x = \eta(\beta_{xx}k_x + \beta_{xy}k_y + \alpha_{xz}k'), \tag{8a}$$

$$v_y = \eta(\beta_{yx}k_x + \beta_{yy}k_y + \alpha_{yz}k'), \tag{8b}$$

$$v_z = \eta(\alpha_{zz}k'), \tag{8c}$$

$$\begin{bmatrix} v_{x'} \\ v_{y'} \\ v_{z'} \end{bmatrix} = \mathbf{O}_3 \begin{bmatrix} v_x \\ v_y \\ v_z \end{bmatrix}. \tag{9}$$

So, we can express the components of the wavevector as (by setting $v_x = 0$)

$$k' = \left\{\left(\frac{2}{\eta^2}\right)\frac{E - V(z)}{f^2\beta_{xx} + 2ef\beta_{xy} + e^2\beta_{yy} + \alpha_{zz}}\right\}^{1/2}, \tag{10}$$

$$e = \frac{\beta_{xx}(\alpha_{zz}\tan\theta - \alpha_{yz}) + \alpha_{xz}\beta_{yx}}{\beta_{xx}\beta_{yy} - \beta_{xy}\beta_{yx}}, \tag{11a}$$

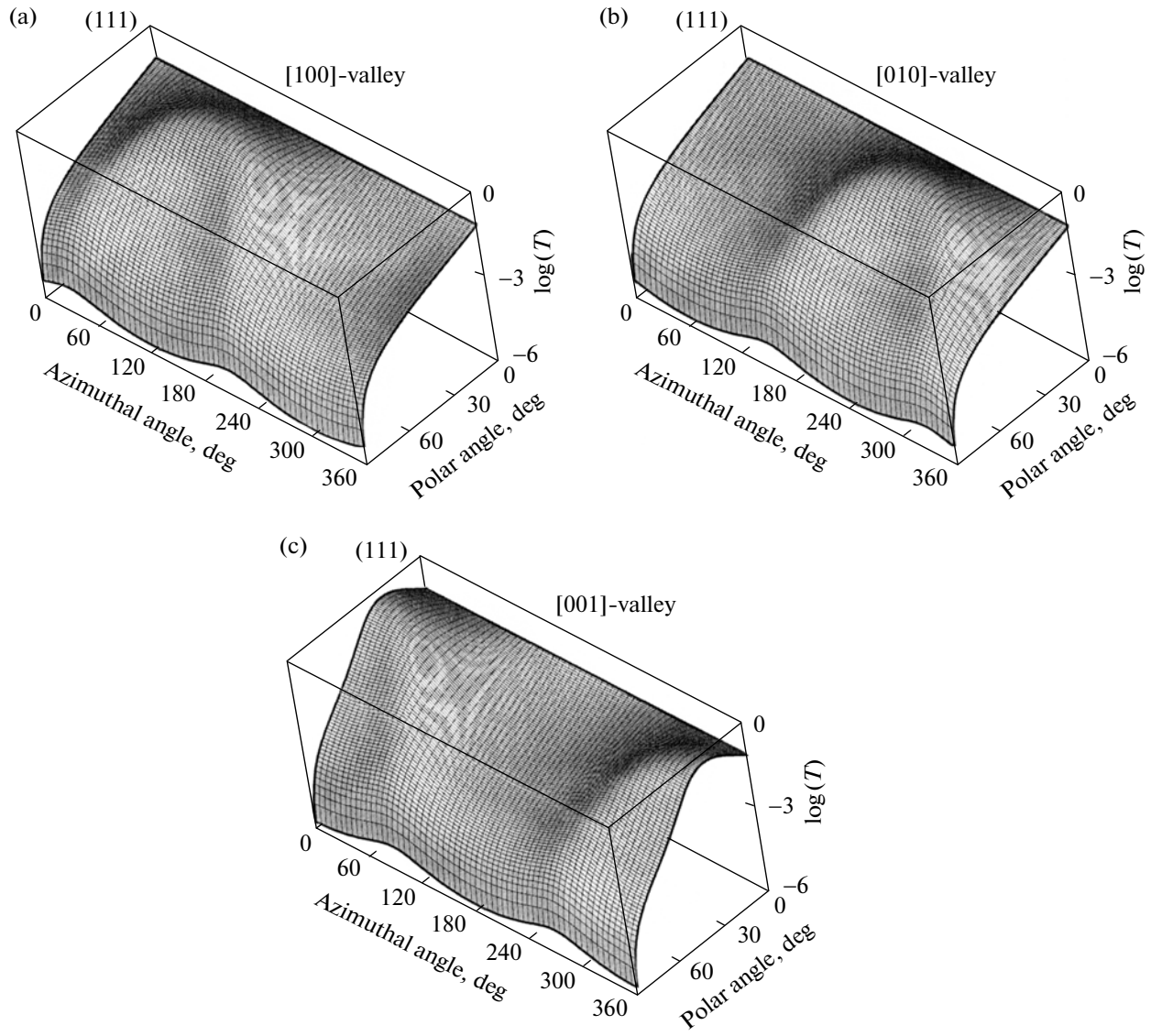

Fig. 2. Calculated transmission coefficients T in (111)-oriented Si rectangular potential barrier generated by incident electrons derived from (a) [100]-, (b) [010]-, and (c) [001]-valleys with different incident angles ($\theta = 0$–$90°$ and $\phi = 0$–$360°$).

$$f = \frac{\beta_{xy}(\alpha_{yz} - \alpha_{zz}\tan\theta) - \alpha_{xz}\beta_{yy}}{\beta_{xx}\beta_{yy} - \beta_{xy}\beta_{yx}}, \quad (11b)$$

$$k_x = fk', \quad (12a)$$

$$k_y = ek', \quad (12b)$$

$$k_z = k' - \gamma, \quad (12c)$$

$$\begin{bmatrix} k_{x'} \\ k_{y'} \\ k_{z'} \end{bmatrix} = \mathbf{O}_3 \begin{bmatrix} k_x \\ k_y \\ k_z \end{bmatrix}. \quad (13)$$

Furthermore, the angle (θ', ϕ') of the wavevector $\mathbf{k}$ can be expressed as

$$\theta' = \cos^{-1}(k_{z'}/\sqrt{k_{x'}^2 + k_{y'}^2 + k_{z'}^2}), \quad (14a)$$

$$\phi' = \tan^{-1}(k_{y'}/k_{x'}). \quad (14b)$$

3. RESULTS AND DISCUSSION

In the indirect-gap semiconductors, the conduction electrons occupy valleys with ellipsoidal constant-energy surfaces (ellipsoids). For the layer of a device structure grown on an anisotropic material (ellipsoidal valleys), there are non-zero off-diagonal elements in the effective-mass tensor when one or

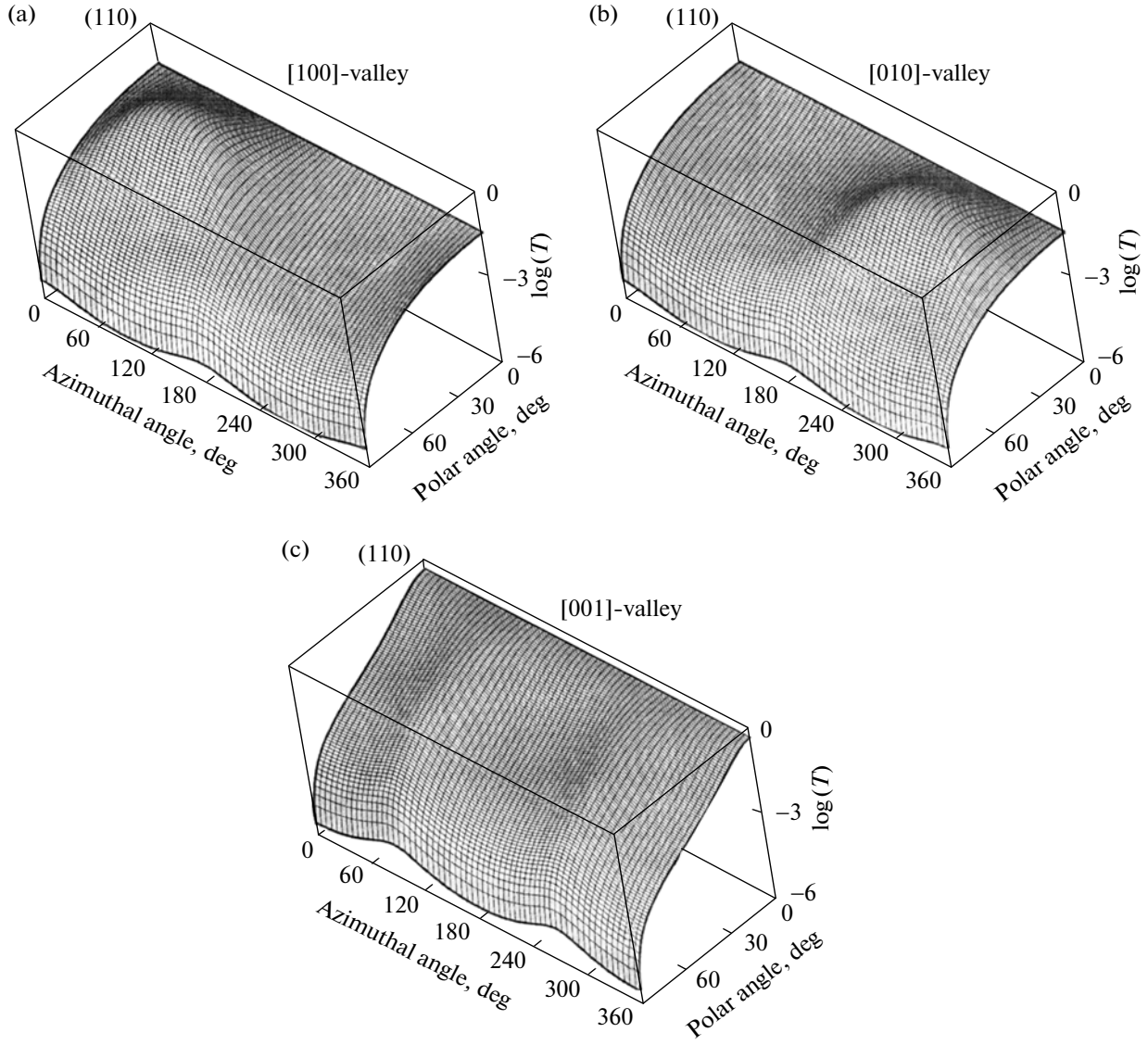

Fig. 3. Calculated transmission coefficients T in (110)-oriented Si rectangular potential barrier generated by incident electrons derived from (a) [100]-, (b) [010]-, and (c) [001]-valleys with different incident angles ($\theta = 0$–$90°$ and $\phi = 0$–$360°$).

more of principal axes of the ellipsoids is tilted with respect to growth direction, as proven in the Appendix A.

The energy coupling effects of the longitudinal motion to the transverse motion exists in anisotropic materials via the off-diagonal effective-mass tensor elements. And, the off-diagonal effective-mass tensor elements are valley dependent, which suggests that the coupling effects are not identical in all valleys. The coupling strength between the transverse and longitudinal motions varies with the in-plane angle and growth-direction because of the different off-diagonal effective-mass tensor elements; and it implies the loss or gain of kinetic energy for longitudinal direction, helping or hindering the tunneling on a potential barrier. Thus, it is necessary to investigate its effect on the tunneling quite rigorously.

From Eqs. (10)–(13), we can obtain the components of the wavevector (k_i, $i = x', y', z'$) in an anisotropic material when the energy (E) and velocity angle (θ, ϕ) of the incident electron are known. Moreover, we can also obtain the relation between the **k** direction (θ', ϕ') and v direction (θ, ϕ) in an anisotropic material through the simulation and calculation of Eqs. (10)–(14). Owing to the existing of the non-zero off-diagonal elements in the effective-mass tensor, it should be noted that **k** and **v** are not necessarily parallel in an anisotropic material, as shown in Eq. (8).

We previously had derived the non-equilibrium Green's function method for a quantum-transport

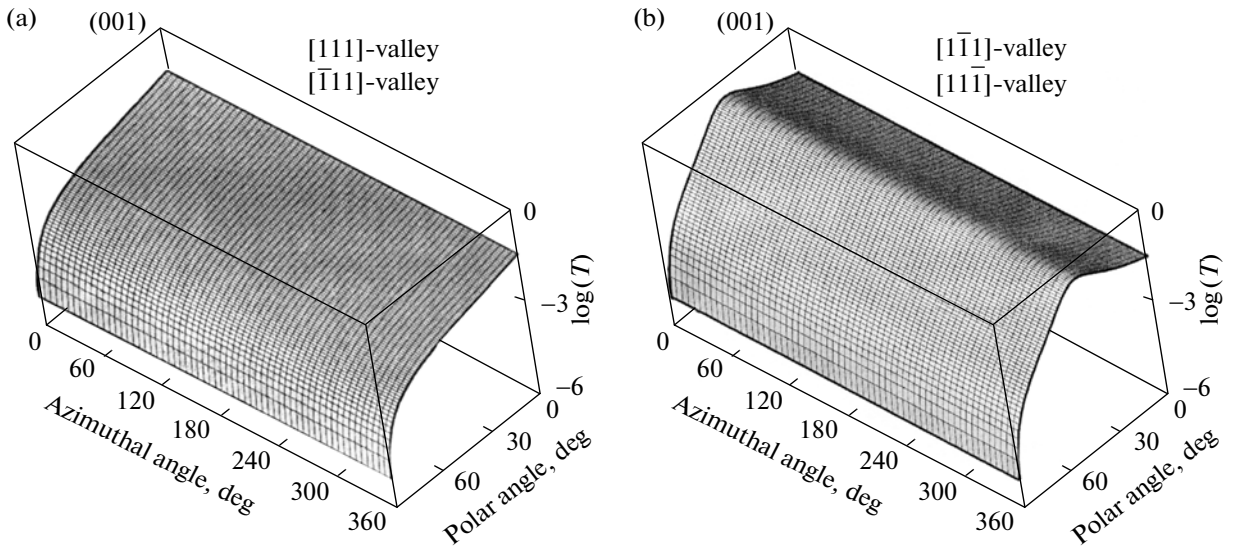

Fig. 4. Calculated transmission coefficients T in (001)-oriented Ge rectangular potential barrier generated by incident electrons derived from (a) [111]- and [$\bar{1}$11]-valleys and (b) [1$\bar{1}$1]- and [11$\bar{1}$]-valleys with different incident angles ($\theta = 0$–$90°$ and $\phi = 0$–$360°$).

calculation on anisotropic materials and successfully calculated the transmission coefficient of an electron through a potential barrier [12]. In this study, as an extension to this, we calculate the velocity-direction dependent transition coefficient of an incident electron through a potential barrier grown on an anisotropic material.

In this study, a rectangular potential barrier with barrier thickness $d = 30$ nm and barrier height $V_0 = 200$ meV is considered as an example for (001)-, (111)-, and (110)-orientations. It should be noted that the rectangular barrier approximates to a source-to-drain Si or Ge potential barrier of MOSFETs.

In X-valley material (Si), the 6 equivalent minima of the conduction band are located at the X points of the Brillouin zone. For Si (001), $\hat{x}'$, $\hat{y}'$, and $\hat{z}'$ are chosen along the [100], [010], and [001] directions, respectively. For a Si (001) surface there are 2 systems: a system which is two-fold degenerate valleys (X2), [001]- and [00$\bar{1}$]-valleys, with their small effective mass in the z'-direction, and a system which is four-fold degenerate valleys (X4). Owing to the X2 valleys with smaller effective mass in the z'-direction, the transmission coefficients of the X2 valleys are larger than those of the X4 valleys under norma-incident ($\theta = 0°$), as shown in Fig. 1. Furthermore, the transmission coefficients of the X2 valleys are in-plane angle (ϕ) independent, and also for the X4 valleys.

For Si (111), $\hat{x}'$, $\hat{y}'$, and $\hat{z}'$ are defined along the [11$\bar{2}$], [$\bar{1}$10], and [111] directions, respectively. For the Si (111) growth direction, the X valleys do not split due to the symmetry of X valleys with respect to the structure coordinate system (x', y', z'). For a Si (111) surface, however, the effective mass along the z'-direction is equal for all six valleys. In that case only one six-fold degenerate system exists. The 6 conduction bands are equivalent on the Si (111) surface. Therefore, the transmission coefficients of six equivalent valleys are the same, but the in-plane phase difference of these valleys is $\phi = 120°$, as shown in Fig. 2.

For Si (110), $\hat{x}'$, $\hat{y}'$, and $\hat{z}'$ are chosen along the [00$\bar{1}$], [$\bar{1}$10], and [110] directions, respectively. For the Si (110) growth direction, the six X valleys are split into doublet [001] and [00$\bar{1}$] valleys (X2) and other four-fold degenerate valleys (X4). The X4 effective mass of Si (110) is different from that of X4 ellipsoids in Si (001). For Si (110) with 6 energy ellipsoids, 4 of them (X4) are tilted toward the growth direction, [110], resulting in the non-vanishing off-diagonal elements in the effective-mass tensor. The effective-mass anisotropy of electrons in these valleys can provide coupling between the parallel and perpendicular motions of the electrons. As shown in Figs. 3a and 3b, the transmission coefficients of X4 valleys are the same, but the in-plane phase difference of these valleys are $\phi = 180°$. Figure 3c exhibits that the largest transmission coefficients in Si (110) are located in the X2 valleys near $\theta = 0$.

The indirect conduction valleys of Ge are located at the conduction band minimum at L point. Ge (001) has four (or half of eight) energy ellipsoids at L points and the ellipsoids are titled toward the growth direction, [001]. Especially, the transmission coefficients of the L valleys are in-plane angle (ϕ) independent, as

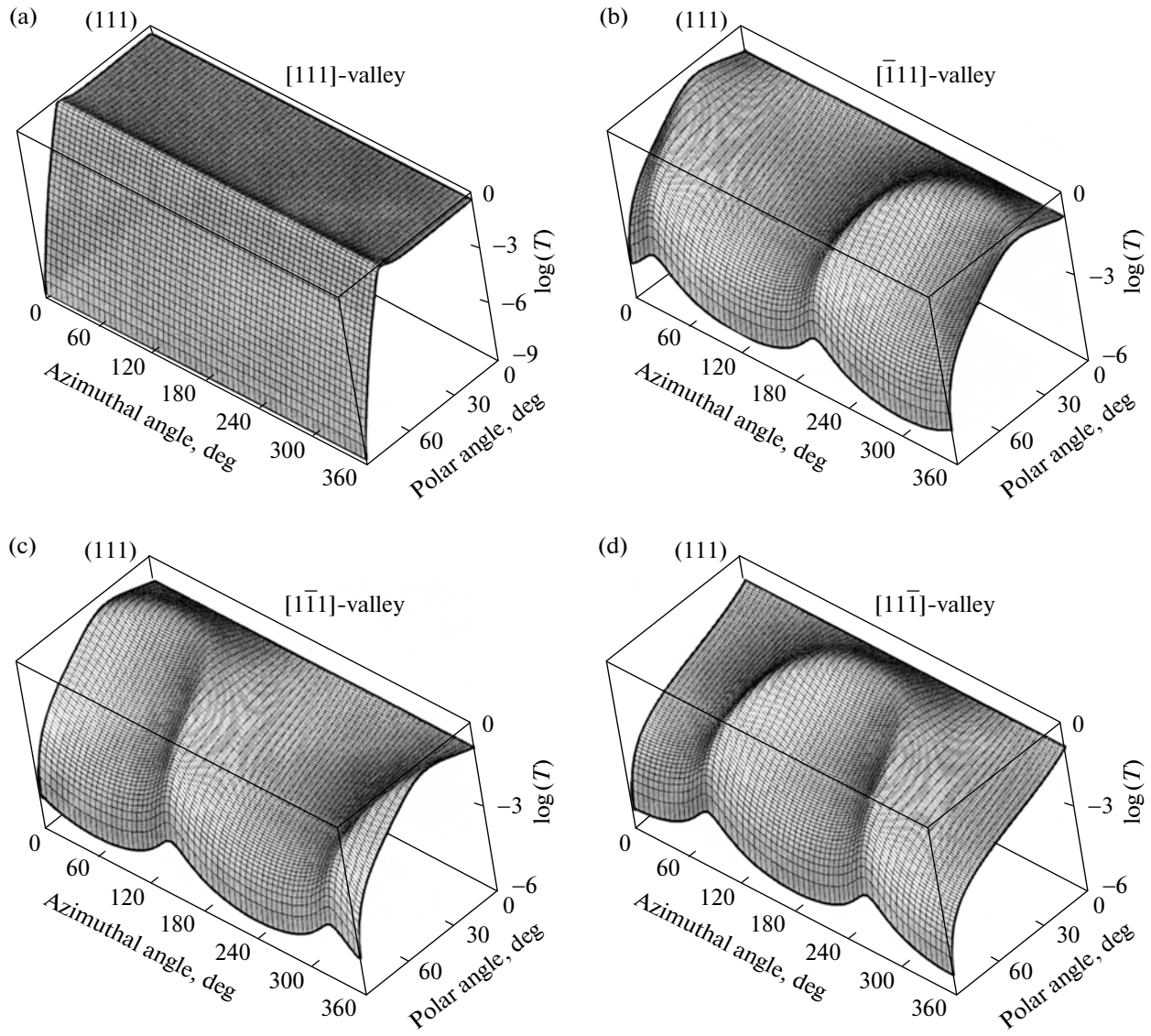

Fig. 5. Calculated transmission coefficients T in (111)-oriented Ge rectangular potential barrier generated by incident electrons derived from (a) [111]-, (b) [$\bar{1}$11]-, (c) [1$\bar{1}$1], and (d) [11$\bar{1}$]-valleys with different incident angles ($\theta = 0$–$90°$ and $\phi = 0$–$360°$).

shown in Fig. 4. Figure 4b exhibits that the largest transmission coefficients in Ge (001) are located at the [1$\bar{1}$1]- and [11$\bar{1}$]-valleys near $\theta = 40°$.

For the growth on (111) substrates, the L valleys split into a singlet [111] valley and triplet degenerate valleys along the [$\bar{1}$11], [1$\bar{1}$1], and [11$\bar{1}$] directions, whose energy ellipsoids of the triplet valleys are tilted with respect to the growth direction, resulting in the non-vanishing off-diagonal elements in the effective-mass tensor. Figure 5a shows that the largest transmission coefficients in Ge (111) are located at the singlet [111]-valley near $\theta = 0$. As shown in Figs 5b, 5c, and 5d the transmission coefficients of triplet degenerate valleys are the same, but the in-plane phase difference of these valleys is $\phi = 120°$.

For Ge (110), the four L conduction band valleys are symmetrically equivalent. However, the effective-mass tensor elements of these four valleys are not the same. As shown in Figs. 6a and 6d, the transmission coefficients of [111]- and [11$\bar{1}$]-valleys are the same, but the in-plane phase difference of the two valleys is $\phi = 180°$. As shown in Figs. 6b and 6c, the transmission coefficients of [$\bar{1}$11]-and [1$\bar{1}$1]-valleys are the same, but the in-plane phase difference of the two valleys is near $\phi = 90°$. Furthermore, Figs. 6b and 6c show that the largest transmission coefficient in Ge (110) are located at the [$\bar{1}$11]- and [1$\bar{1}$1]-valleys near $\theta = 0°$.

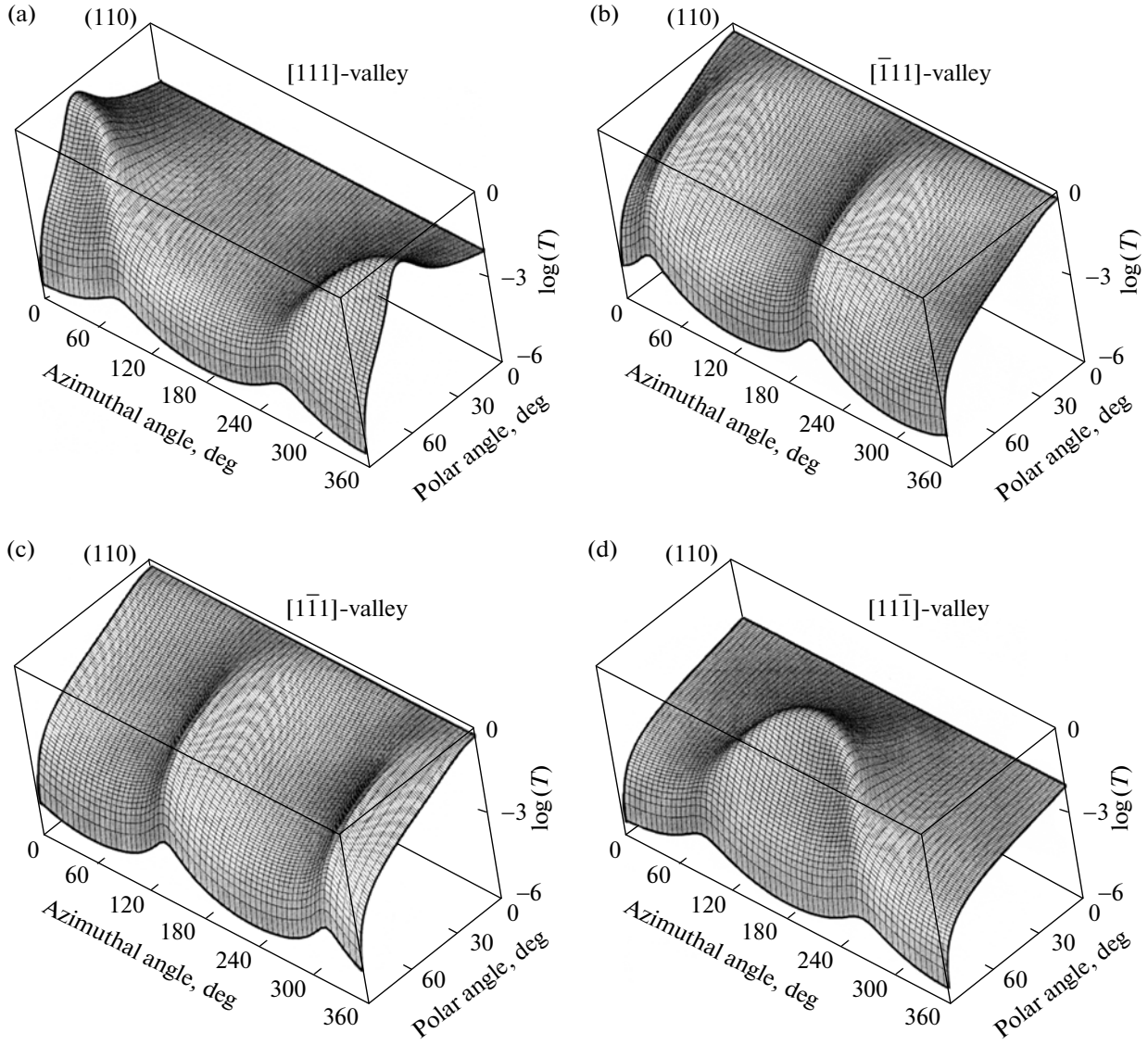

Fig. 6. Calculated transmission coefficients T in (110)-oriented Ge rectangular potential barrier generated by incident electrons derived from (a) [111]-, (b) [$\bar{1}$11]-, (c) [1$\bar{1}$1], and (d) [11$\bar{1}$]-valleys with different incident angles ($\theta = 0$–$90°$ and $\phi = 0$–$360°$).

4. CONCLUSIONS

In anisotropic semiconductors, the mathematical equations of the electron wavevector have been derived and expressed as a function of the velocity-angle and energy of incident electron. Through a potential barrier grown on (001)-, (111)-, and (110)-oriented anisotropic semiconductors, the velocity-direction dependent transition coefficients of an incident electron have been calculated in all valleys and incident-directions. The results have showed that the transition coefficients are strongly incident-direction and valley dependent. The results are suitable for the design guideline of device and contact geometric-shape in the ballistic devices.

APPENDIX

In general situation, the growth direction $\hat{z}'$ of a sample is along the $[hk\lambda]$ direction, while the major axis of an ellipsoidal valley is along the $[mnp]$ direction. In the above depiction, the 3×3 reciprocal effective mass tensor W_{ij} (with $i, j = x', y', z'$) is given by [9, 26].

$$\begin{bmatrix} W_{x'x'} & W_{x'y'} & W_{x'z'} \\ W_{y'x'} & W_{y'y'} & W_{y'z'} \\ W_{z'x'} & W_{z'y'} & W_{z'z'} \end{bmatrix} = \mathbf{O}_1^T \mathbf{O}_2 \begin{bmatrix} w_t & 0 & 0 \\ 0 & w_t & 0 \\ 0 & 0 & w_l \end{bmatrix} \mathbf{O}_2^T \mathbf{O}_1, \quad \text{(A.1)}$$

where $w_t = 1/m_t$, $w_l = 1/m_l$, m_t and m_l are the transverse and longitudinal effective masses, of ellipsoidal valley,

respectively, T denotes the transpose of the matrices, and $\mathbf{O}_{1(2)}$ are the rotational matrices, which are given by

$$\mathbf{O}_\zeta = \begin{bmatrix} \cos\Omega_\zeta\cos\omega_\zeta & -\sin\omega_\zeta & \sin\Omega_\zeta\cos\omega_\zeta \\ \cos\Omega_\zeta\sin\omega_\zeta & \cos\omega_\zeta & \sin\Omega_\zeta\sin\omega_\zeta \\ -\sin\Omega_\zeta & 0 & \cos\Omega_\zeta \end{bmatrix} \quad (\zeta = 1 \quad \text{or} \quad 2), \tag{A.2}$$

with

$$\Omega_1 = \tan^{-1}(\sqrt{h^2 + k^2}/\lambda), \tag{A.3}$$

$$\omega_1 = \tan^{-1}(k/h), \tag{A.4}$$

$$\Omega_2 = \tan^{-1}(\sqrt{m^2 + n^2}/p), \tag{A.5}$$

$$\omega_2 = \tan^{-1}(n/m). \tag{A.6}$$

ACKNOWLEDGMENTS

This work was supported in part by National Science Council (NSC), Taiwan under Contract NSC-99-2112-M-032-006 and NSC-97-2221-E-009-154-MY2.

REFERENCES

1. N. Arora, *MOSFET Modeling for VLSI Simulation: Theory and Practice* (Workd Scientific, Singapore, 2007).
2. A. B. Bhattacharyya, *Compact MOSFET Modeling for VLSI Design* (Wiley, Singapore, 2009).
3. A. Rahman, J. Guo, S. Datta, and M. Lundstrom, IEEE Trans. Electron. Dev. **50**, 1853 (2003).
4. J. H. Rhew and M. S. Lundstrom, J. Appl. Phys. **92**, 5196 (2002).
5. J. Wang and M. Lundstrom, IEEE Trans. Electron. Dev. **50**, 1604 (2003).
6. E. O. Kane, in *Semiconductors and Semimetals,* Ed. by R. K. Willardson and A. C. Beer (Academic Press, New York, 1966), vol. 1, p. 75.
7. J. Luttinger and W. Kohn, Phys. Rev. **97**, 869 (1955).
8. J. Luttinger, Phys. Rev. **102**, 1030 (1955).
9. C. N. Chen, Phys. Rev. B **72**, 085305 (2005).
10. S. Datta, Superlatt. Microstruct. **28**, 253 (2000).
11. Z. Ren, R. Venugopal, S. Goasguen, S. Datta, and M. S. Lundstrom, IEEE Trans. Electron. Dev. **50**, 1914 (2003).
12. C. N. Chen, W. L. Su, M. E. Lee, J. Y. Jen, and Yiming Li, Jpn. J. Appl. Phys. pt. 2 **50**, 060201 (2011).
13. K. Y. Kim and B. Lee, Phys. Rev. B **58**, 6728 (1998).
14. K. Y. Kim and B. Lee, Superlatt. Microstruct. **24**, 389 (1998).
15. R. A. Abram and M. Jaros, *Band Structure Engineering in Semiconductor Microstucture* (Plenum Press, New York, 1989).
16. R. H. Henderson and E. Towe, J. Appl. Phys. **79**, 2029 (1996).
17. Y. Kajikawa, J. Appl. Phys. **86**, 5663 (1999).
18. J. H. Park, D. Kuzum, H. Y. Yu, and K. C. Saraswat, IEEE Trans. Electron. Dev. **58**, 2394 (2011).
19. J. Zhuge, A. S. Verhulst, W. G. Vandeberghe, W. Dehaene, R. Huang, Y. Wang, and G. Groeseneken, Semicond. Sci. Technol. **26**, 085001 (2011).
20. J. Appenzeller, J. Knoch, M. T. Bjork, H. Riel, H. Schmid, and W. Riess, IEEE Trans. Electron. Dev. **55**, 2827 (2008).
21. J. Guo and M. S. Lundstrom, IEEE Trans. Electron. Dev. **49**, 1897 (2002).
22. Q. T. Zhao, J. M. Hartmann, and S. Mantl, IEEE Electron. Dev. Lett. **32**, 1480 (2011).
23. C. H. Shih and N. D. Chien, IEEE Electron. Dev. Lett. **32**, 1498 (2011).
24. K. Yamamoto, R. Ueno, T. Yamanaka, K. Hirayama, H. Yang, D. Wang, and H. Nakashima, Appl. Phys. Express **4**, 051301 (2011).
25. N. Taoka, W. Mizubayashi, Y. Morita, S. Migita, H. Ota, and S. Takagi, J. Appl. Phys. **108**, 104511 (2010).
26. C. N. Chen, J. Appl. Phys. **97**, 113704 (2005).